Organic N-type Electrets for Field-effect Transistors, Photo Memories and Artificial Synapses

Dongfan Li
　Xi'an Jiaotong University

Zongze Qin
　Xi'an Jiaotong University

Wanlong Lu
　Xi'an Jiaotong University

Yurong Ren
　Xi'an Jiaotong University

Yuanwei Zhu
　Xi'an Jiaotong University

Hong Wang
　Xi'an Jiaotong University　https://orcid.org/0000-0002-7989-1672

Shengtao Li
　Xi'an Jiaotong University

Laju Bu
　Xi'an Jiaotong University

Guanghao Lu (✉ guanghao.lu@mail.xjtu.edu.cn)
　Xi'an Jiaotong University　https://orcid.org/0000-0001-7829-7308

Article

Organic N-type Electrets for Field-effect Transistors, Photo Memories and Artificial Synapses

ABSTRACT: Electrets, typically referring to insulator materials with permanently-trapped charges, are widely used for electronic devices, actuators and medical filtering. Here, organic n-type electrets, generated from oxygen-degraded n-type semiconductors, are proposed as photo-induced electrets. The sheet charge densities of such n-type electret films, as high as 7.47×10^{12} cm^{-2}, are used to provide steady built-in electric field to significantly improve the performance of organic field-effect transistors (OFETs). For example, OFETs made of p-type semiconductor 2,7-dioctyl[1]benzothieno[3,2-b][1]benzothiophene (C$_8$-BTBT), in combination with n-type electret N,N ′ -Dioctyl-3,4,9,10-perylenedicarboximide (C$_8$-PTCDI), show a hole field-effect mobility 13.3 cm^2·V^{-1}·s^{-1}, along with a memory window over 100 V, a memory on/off ratio 10^6 and a stable retention life time over one month in ambient air. Subsequently, the generality of n-type electrets for transistors and photo memories applications are demonstrated. Furthermore, OFETs with organic n-type electrets are employed in artificial synapse, and the recognition rate of brain-inspired neuromorphic computing is 65%.

INTRODUCTION

Insulator materials with quasi-permanently trapped charges are generally named as insulator electrets[1], which are widely used in transistors[2], nanogenerators[3-4], energy harvesters[5], microphones[6] and filters[7]. For example, organic field-effect transistors (OFETs) are attracting sustainable interests for low-cost flexible electronics[8]. Typically, OFETs require high field-effect mobility, large on/off ratio, tunable threshold voltage, steep subthreshold swing, and good stability. To improve OFETs performance, insulator electrets, as an "container" for trapping neat charges, provide built-in electric field to manipulate the accumulation and depletion of mobilized charges within semiconductor layer, and thus to tune the charge transport in semiconductor layer. In fact, insulator electrets are not only used to manipulate threshold voltage[9], but also contribute to improving on/off ratio of OFETs[10]. Moreover, with the built-in inhomogeneous electric field, provided by inhomogeneous insulator electrets, the measured field-effect mobility is improved, with optimized subthreshold swing[11].

However, as compared with metal or semiconductor, insulator materials are simultaneously featured with low electron affinity potential (for electron storing) and high ionization potential (for hole storing), which means that the trapped charges are energetically unfavorable, tending to leak away. Moreover, the intrinsic low mobility of carriers in insulators implies that charge injection into the insulator requires substantial time- and/or energy-consuming, for example, by high voltage or at high temperature[12-13]. On the other hand, chemical dopants with suitable electron affinity or ionization potential provide alternative hosts for stable charge storage[14]. However, the

chemical doping induced charge transfer from semiconductors to dopants is typically irreversible and usually independent on external stimulations (for example, light illumination), which thus is not easily applicable to electronic switches or memory devices.

Taking above considerations into account, in this work we propose a class of new electrets, namely oxygen-degraded n-type semiconductors. That is, after degradation by oxygen species, the n-type semiconductors become electrically insulating and charging of this "insulating" electret can be realized by light illumination, which endows the n-type electret with a unique characteristic as a photo-induced electret.

Actually, the oxidation of p-type semiconductors with high ionization potential usually induces extra holes to fill the traps, contributing to a higher electrical conductivity[9]. On the contrary, the oxidation induced degradation of n-type semiconductors typically induces new traps to immobilize electron carriers, significantly decreasing the electron mobility. Although these oxygen-degraded n-type semiconductors typically show several orders of magnitude lower electron mobility than the undegraded materials, their electrons affinities are almost kept and thus can stably accommodate sufficient trapped electrons. Consequently, this work provides an easily-accessible method to generate photo-induced organic n-type electrets, showing wide applications in OFETs, photo memories and artificial synapses.

RESULTS AND DISCUSSION

In this work, oxygen-degraded N,N'-dioctyl-3,4,9,10-perylene diimide (C_8-PTCDI) is taken as an example for n-type electret (Fig. 1). For clarity, we use a n-type

semiconductor/p-type semiconductor (n/p) heterojunction architecture for OFETs application, while p-type semiconductor is 2,7-diocty[1]benzothieno[3,2-b][1]benzothiophene (C_8-BTBT). The photoresponsive behavior of OFETs is commonly realized by photo-induced charge transfer from donor into the acceptor[15-16]. This behavior actually involves two processes including the electron excitation and charge transfer. Take n/p heterojunction of C_8-PTCDI/C_8-BTBT as an example. When the photons are absorbed by C_8-BTBT molecules, the electrons are photo-excited from the highest occupied molecular orbit (HOMO) into the lowest unoccupied molecular orbit (LUMO), leaving holes in the HOMO and excitons are thus formed[17]. Then, the electric field, provided by the energy offset between the C_8-BTBT donor and C_8-PTCDI acceptor, affords a driving force for exciton separation. That is, the electrons excited into LUMO level of C_8-BTBT are transferred to the LUMO level of C_8-PTCDI (Fig. 1a). After light illumination, C_8-PTCDI and C_8-BTBT obtains equal number of electrons and holes, respectively. The increase of hole concentrations in C_8-BTBT after light illumination improves drain current (I_{ds}) of the OFETs, which refers to the well-known photoconductivity. However, due to the intrinsic electron mobility of C_8-PTCDI, the electrons tend to be instable under external stimulus (e.g. the sweep of gate voltage, V_{gs}), and finally are extracted from C_8-PTCDI. The abovementioned instability makes C_8-PTCDI a poor container for storing electrons, failing to act as the conventional electrets to stably supply built-in electric field to well regulate the accumulation or depletion of holes in the semiconducting layer. Consequently, the photoconductivity,

which is a characteristic of such a n/p heterojunction, is actually not maximally achieved[18].

Here, an easily accessible and repeatable method is proposed to suppress the unintended electron extraction from the C_8-PTCDI molecules by utilizing the oxygen-induced degradation. In fact, most organic semiconductors can be gradually degraded by the ambient oxygen, especially for n-type semiconductors, leading to a significant decrease of electrical conductivity due to the formation of numerous traps[19-20]. This is the well-known ambient degradation of organic electronics. However, the much lower electron mobility of degraded n-type semiconductors enables themselves as good organic n-type electret materials for stably storing electrons, and the n-type electrets provide sustainable built-in electric field to effectively tune the accumulation of holes in the conductive channel. In a word, the electrons, photo-excited from C_8-BTBT, are transferred and stably trapped (immobilized) inside the degraded C_8-PTCDI. These trapped electrons inside C_8-PTCDI, namely organic n-type electrets, provide additional electric field to to the gate-voltage-induced field and regulate the accumulation or depletion of holes in C_8-BTBT (Fig. 1b), and thus the photoconductivity of OFETs are boosted and the conductivity can be kept for a longer time. Coincidentally, the oxidation-boosted charge trapping is recently reported in InSe field-effect transistors[21], demonstrating that the degradation of semiconductors shows practical applications in electronic devices.

The bottom-gate top-contact OFETs with n/p heterojunction are demonstrated in

Fig. 1a. The nominal layered interface of n/p heterojunction is in fact roughly presented, due to the polycrystalline feature of organic semiconductors[18]. Therefore, although C_8-PTCDI was deposited on C_8-BTBT layer via thermal evaporation, at the interface, the n-type semiconductors are actually partly mixed with the p-type semiconductors[22]. Moreover, the nominal thickness of n-type semiconductors is crucial for the device performance. That is, the OFETs show substantial off-state current when the thickness of C_8-PTCDI is over 2 nm (Supplementary Fig. 1). This can be explained by the effective electron transport through the interconnected network of n-type semiconductors. Therefore, the following 40 nm C_8-BTBT-based OFETs, in combination with 2 nm n-type semiconductor, were fabricated unless specified. In a word, the top surface of the mixed semiconductors film is not always n-type semiconductors, and this key point will be referred later.

To further validate the generality of organic n-type electrets, different p-type conjugated polymer poly[4-(4,4-dihexadecyl-4H-cyclopenta[1,2-b:5,4-b′]-dithiophen-2-yl)-alt-[1,2,5]thiadiazolo[3,4-c]pyridine] (PCDTPT) in combination with C_8-PTCDI, and C_8-BTBT-based OFETs with different degraded n-type semiconductors of [6,6]-phenyl-C71-butyric acid methyl ester ($PC_{71}BM$) and (N,N′-bis(n-octyl)-1-bromoperylene- 1,4,5,8-bis(dicarboximide) (Br-NDI) were simultaneously investigated. It is noted that the OFETs performance is poor when naked SiO_2 without any modification is used as the dielectric layer[9]. Therefore, atactic poly(4-fluorostyrene) (FPS) and polystyrene (PS), acting as a passivation layer, are both used to modify the

surface of SiO_2, respectively. And their molecular structures are shown in Supplementary Fig. 2.

Subsequently, in-situ degradation of n-type semiconductors and quantitative analyses of degradation-dependent photoconductivity of OFETs with n/p configuration are both investigated. To in-situ degrade the OFETs fabricated with pure C_8-PTCDI, five strategies including air exposure (with and without heating), oxygen plasma (low and high pressure) and ozone are adopted. The maximum I_{ds} and on/off ratio are decreased by over an order of magnitude and over two orders of magnitude, respectively, after exposure to open air for over 100 days (Supplementary Fig. 3a). When OFETs were annealed at 120 °C in ambient conditions, the degradation of C_8-PTCDI is accelerated (Supplementary Fig. 3b). Compared with oxygen doping in the ambient, high-pressure (150 Pa) oxygen plasma could easily deteriorate C_8-PTCDI and the maximum I_{ds} is significantly decreased in 30 s (Supplementary Fig. 3c). Basically, longer durations of plasma treatment should further increase the on-state current. However, plasma could also etch the organic films,[9] which is thus uncontrollable to reserve enough C_8-PTCDI molecules in C_8-BTBT. For low-pressure (30 Pa) oxygen plasma treatment, doping efficiency is limited (Supplementary Fig. 3d).

Ozone, as a mild way to react with organic films, could effectively deteriorate the electron charge transport in n-type semiconductor molecules, which refers to degradation of n-type semiconductors. Therefore, I_{ds} is reduced by two orders of magnitude in a few minutes (Fig. 2a). Therefore, in the following investigation, ozone

is used as a model oxygen species in this work unless specified. Atomic Force Microscopy topographies (Fig. 2b-c) show minor changes in roughness as well as the morphology of semiconductor films after ozone treatment. Infrared (Fig. 2d) and ultra violet-visible (UV-vis) absorption spectra (Fig. 2e) also show little difference after ozone treatment, indicating major molecules are not degraded. Meanwhile, the glass coated by mixed semiconductors films with n/p heterojunction show a good optically transparency over 95% in visible region (Fig. 2f), demonstrating a potential application of n-type electret for transparent electronics. The height profile and transparency of the films are both shown as the inset of Fig. 2f.

To study the HOMO energy level of degraded C_8-PTCDI, ultraviolet photoelectron spectroscopy spectra are investigated, which actually involves three parameters. That is, incident photon energy (hv = 21.2 eV), high binding energy cutoff (E_{cutoff}) and the onset of degraded C_8-PTCDI thin film relative to the E_F of Au (E_{onset})[23]. From Fig. 2g-h, E_{cutoff} = 17.68 ± 0.02 eV and E_{onset} = 2.46 ± 0.02 eV are obtained, respectively. The HOMO energy is thus calculated according to the following equation:

$$E_{HOMO} = hv - (E_{cutoff} - E_{onset}) \qquad (1)$$

Therefore, for degraded C_8-PTCDI thin film, E_{HOMO} = 5.98 ± 0.04 eV, while the LUMO energy of degraded C_8-PTCDI thin film is:

$$E_{LUMO} = E_{HOMO} - E_g \qquad (2)$$

where E_g is the optical gaps. E_g = 1.98 eV (Fig. 2i) can be obtained from the UV-vis absorption spectra by using Tauc plot[24]. Therefore, E_{LUMO} of 4 ± 0.04 eV and E_{HOMO} of

5.98 ± 0.04 eV are calculated in this work, which is consistent with previous reports[22, 25-26]. Meanwhile, for as-prepared C_8-PTCDI, E_{LUMO} of 4.07 ± 0.06 eV and E_{HOMO} of 6.02 ± 0.06 eV are obtained from Supplementary Fig. 4, demonstrating that the energy levels of the as-prepared C_8-PTCDI and degraded C_8-PTCDI are almost identical.

Actually, the degraded molecules of C_8-PTCDI are solely a minority in terms of whole C_8-PTCDI, which can be used to explain both the lowered electron mobility and unchanged energy levels of degraded C_8-PTCDI. This part will be discussed later. Even though the ratio of degraded molecules is low compared with whole C_8-PTCDI molecules, the electrical conductivity of C_8-PTCDI-based OFETs is significantly decreased after ozone treatment, which is necessary for electret materials. Due to the fact that the energy levels of degraded C_8-PTCDI are almost unchanged, electrons could be spontaneously transferred from C_8-BTBT into degraded C_8-PTCDI by energy offset. On the other hand, poor conductivity makes the degraded C_8-PTCDI could easily carry and store electrons even under cyclic external stimuli (e.g. the sweep of V_{gs} lower than 100 V). These trapped electrons appeal equal number of holes in C_8-BTBT due to the Coulombic interaction. Finally, the electrical conductivity of C_8-BTBT-based OFETs, affected by organic n-type electrets, is significantly enhanced under light illumination, indicating that organic n-type electrets contribute to improving the photoconductivity of OFETs.

In order to verify the role of organic n-type electrets for device applications, OFETs with configuration of C_8-PTCDI/C_8-BTBT is used as an example, and the

relationship between OFETs photoconductivity and degrees of C_8-PTCDI degradation

is quantitatively investigated. For as-prepared OFETs, onset voltage (V_{on}) is positively

shifted from -4 V to 10 V, and the maximum I_{ds}, referring the I_{ds} at V_{gs} = -60 V, is

increased twice in magnitude under light illumination (Fig. 3a), which is a sign of

photoconductivity[27]. To quantitatively evaluate photoconductivity, the shift of onset

voltage (ΔV_{on}) and I_{photo}/I_{dark} ratio will be discussed. That is, ΔV_{on}, the V_{on} discrepancy

of transfer curves measured in the dark and light illumination, is 14 V. I_{photo}/I_{dark} ratio,

the ratio of photocurrent and dark current at a specified V_{gs}, is 1.3×10^5 (Fig. 3a). Here,

I_{photo} and I_{dark} is measured while keeping light on and in the dark, respectively. The

specified V_{gs} is chosen as V_{on}. After C_8-PTCDI molecules are partially degraded, ΔV_{on}

and I_{photo}/I_{dark} ratio is increased to 120 V and 1.8×10^7, respectively (Fig. 3b), indicating

an enhancement of photoconductivity[18]. It is noted that V_{on} is extracted from forward

transfer curves (as arrows shown in Fig. 3b). As the absorption peak of C_8-BTBT is ~

365 nm (Fig. 2e), the wavelength of light source is thus selected as 365 nm unless

specified.

From Fig. 3c, OFETs are demonstrated from accumulation mode to depletion

mode by light illumination, indicating the increase of I_{photo}[28]. In the dark, holes in C_8-

BTBT are extracted under gate electric field, and hole concentrations are thus decreased.

As a result, I_{ds} is low at V_{gs} = 70 V and OFETs are in *off* state. When light illumination

is given, large number of holes, induced by organic n-type electrets, are accumulated in

C_8-BTBT. Therefore, I_{ds} is as high as 50 μA at V_{gs} = 70 V and OFETs are in *on* state.

Meanwhile, I_{photo} in different light intensities (varying from 10 to 850 $\mu W \cdot cm^{-2}$) are investigated, from which I_{photo} is increased with the increase of light intensities (Fig. 3d). This is because the higher light intensity, the more photo-induced excitons are generated per unit time, and thus higher charge densities of organic n-type electrets are formed, leading to higher hole concentrations in C_8-BTBT.

In the following, the relationship between ozone treatment time and ΔV_{on} as well as I_{photo}/I_{dark} ratio are investigated from over 20 devices (Fig. 3e). Initially, ΔV_{on}, as well as I_{photo}/I_{dark} ratio, increases with the increase of ozone treatment time, as longer durations of ozone treatment make more electron trap sites in C_8-PTCDI, and thus more electrons are trapped in organic n-type electrets once light illumination is applied. As a result, the stronger electric field, induced by organic n-type electrets, is bound to accumulate more holes in C_8-BTBT, and thus I_{photo} is increased and meanwhile the transfer curves are shifted towards positive direction. However, ΔV_{on}, as well as I_{photo}/I_{dark} ratio, no longer increase (even decrease) with the further increase of ozone treatment time. This is because longer durations of ozone treatment can damage OFETs performance by over doping[29], which weakened the role of organic n-type electrets.

The fluorescence spectra of 40 nm C_8-BTBT film upon excitation wavelength at 365 nm were investigated, as the absorption peak of C_8-BTBT is $\sim$ 365 nm (Fig. 2e). Compared with absorption peak, the fluorescence peak shows red shift ($\sim$ 372 nm). Compared with pure C_8-BTBT film, the fluorescence intensity of 2 nm degraded C_8-PTCDI/40 nm C_8-BTBT film was quenched (Fig. 3f), indicating these electrons are

efficiently transferred from C_8-BTBT to degraded C_8-PTCDI. This point is reasonable, and can be proved by referring to other systems[16]. Furthermore, Kelvin probe force microscopy (KPFM) was also used to investigate the process of charge transfer. In general, the increase of surface potential is induced by the aggregation of holes or the loss of electrons[30]. The surface potential is increased by light illumination, compared with the initial state (Supplementary Fig. 5), indicating that electrons are efficiently transferred from C_8-BTBT to degraded C_8-PTCDI. From this result, we can conclude that in C_8-BTBT/C_8-PTCDI blend film, C_8-PTCDI is not necessarily located on the top surface, and reasons have been discussed before. In this work, the decay of OFETs photoconductivity is also investigated by measuring the current after exposure OFETs to ambient conditions for several days (Fig. 3b).

In order to make photoconductivity more intuitive, a contour (Fig. 3g) are used, of which the brightness of color is proportional to I_{photo}/I_{dark}. Here, a hollowed flake mask with "X" shape was used to partially filter incident light upon the device with 9×9 array. The mask is placed between light source and device, and mask and device are parallel. First, device with 9×9 OFETs were measured in the dark to obtain I_{dark}. Second, by using the set-up shown in Fig. 3g, I_{photo} was measured one by one under light illumination. By this way, the OFETs located in "X" shape show much larger I_{photo} than those of the others. I_{photo}/I_{dark}, representing brightness level, is then calculated. Afterwards, the above steps are repeated by using hollowed flake masks with "J", "T", "U" shape, respectively. Finally, photoconductivity is represented as the pattern of

"XJTU" (Fig. 3h), and the decay of photoconductivity can be easily read out by the change of "XJTU" pattern after exposure devices to the ambient conditions (Fig. 3i).

By adding n-type electrets, OFETs photoconductivity is markedly improved from both transverse direction (ΔV_{on}) and longitudinal direction (I_{photo}/I_{dark}), providing practical applications of electronic device. In view of transverse direction, OFETs can be used for electrets-based transistor memories. On the other hand, the increase of I_{photo}, from the view of longitudinal direction, can be used as light-responsive sensors and artificial synapses. In the following, the further applications of organic n-type electrets are investigated.

OFETs, with the configuration of C_8-PTCDI/C_8-BTBT/FPS, are used as n-type organic electrets based memories. FPS is used as a passivation layer to modify the surface of bare SiO_2, because OFETs made by using bare SiO_2 show poor performance[9]. For OFETs memories, two key parameters, namely the memory window (V_{MW}) and memory on/off ratio of are defined in Fig. 4a. That is, the shift of transfer curves from programming state to erasing state at $I_{ds} = 10^{-8}$ A is depicted as V_{MW}. Memory on/off ratio, another critical parameter for memory device, is defined as the ratio of I_{ds} of erasing state to programming state at V_{on}.

During programming (V_{gs} = -100 V, 1 s), holes are extracted from C_8-BTBT, and the decrease of hole concentrations result in the decrease of surface potential (Supplementary Fig. 5). Therefore, higher operational voltage is required to drive the OFETs, and V_{on} is shifted from 0 V to ~-55 V (Fig. 4a). In general, holes are injected

into insulators under gate electric field[31]. On special occasions such as in the case of quantum well-like heterojunction, holes are transferred from p-type semiconductor to n-type semiconductor under gate electric field.[16] In this work, both the two routes are involved. That is, partial holes are injected into FPS, and the others are transferred to C_8-PTCDI. The duration of programming operation is short, therefore, current difficulties of practical electrets-based OFETs memories focus on the reverse operation of programming, namely the erasing operation, which is used to accumulate the holes in C_8-BTBT. In detail, one of the difficulties is the delay of electron transport, resulting in relatively longer durations of erasing operation. On the other hand, the electrons trapped in C_8-PTCDI is not stable, leading to relatively lower V_{MW}. To address these issues, three strategies including V_{gs} (+100 V), light illumination, and V_{gs} (+100 V) & light illumination for erasing operation, upon OFETs with and without ozone treatment, are investigated as follows.

Longer gate stress time guarantees that sufficient electrons are injected from source/drain electrodes into C_8-PTCDI and FPS, resulting in the formation of organic n-type electrets and insulator electrets. Additional electric field, provided by the electrets, is bound to increase the hole concentrations in C_8-BTBT, and the surface potential is thus increased after applying positive voltage (Supplementary Fig. 5). The increase of hole concentrations in C_8-BTBT indicates that relatively lower operational voltage can make the OFETs work. In other words, V_{on} is manipulated and V_{MW} is increased with the increase of gate stress time (Supplementary Fig. 6a). On the other

hand, longer durations of light illumination (Supplementary Fig. 6b) or higher intensity of light illumination (Supplementary Fig. 6c) is bound to generate more photo-induced excitons per unit time, and thus more electrons are trapped in C_8-PTCDI. The additional electric field, provided by the organic n-type electrets, largely increases the hole concentrations in C_8-BTBT, and thus V_{MW} is increased with the increase of longer durations of gate stress and light illumination, or light illumination with higher intensity. In a word, the increase of V_{MW} is correlated with the increase of trapped electrons in electrets. The third strategy, synergistically using positive V_{gs} & light illumination for erasing operation, shows advantages, which will be discussed later.

After the in-situ degradation of C_8-PTCDI molecules, V_{MW} becomes larger without degrading memory on/off ratio by positive V_{gs} (Supplementary Fig. 6d) and light illumination (Supplementary Fig. 6e-f) because more electrons are relatively stably trapped in degraded C_8-PTCDI, resulting in the further increase of hole concentrations. As has been mentioned above, both the two routes are occurred during programming operation, in terms of the OFETs configuration with n/p heterojunction. Similarly, in the case of erasing operation by positive V_{gs}, electrons, from source/drain electrodes, were partially injected into n-type semiconductors[16], while the others were transferred into insulator materials[31], which suffers from long durations[9, 31]. In other words, the number of electrons, transferred in insulator materials, is limited in short time. Therefore, most electrons were injected into degraded C_8-PTCDI, as V_{MW} is increased from 16 V (Supplementary Fig. 6a, as-prepared OFETs) to 67 V (Supplementary Fig.

6d, OTETs pre-treated by ozone) in 1 s. Meanwhile, in the case of erasing operation by light illumination for 1 s, V_{MW} is increased from 50 V/52 V (Supplementary Fig. 6b, Supplementary Fig. 6c, as-prepared OFETs) to 97 V/91 V (Supplementary Fig. 6e, Supplementary Fig. 6f, OTETs were pre-treated by ozone), indicating electrons were transferred from C_8-BTBT to C_8-PTCDI. Therefore, in the case of erasing operation, most electrons are trapped in degraded C_8-PTCDI. Consequently, the increase of V_{MW} is correlated with the increase of trapped electrons in organic n-type electrets.

As for synergistically using positive V_{gs} & light illumination, V_{MW} is boosted from 55 V (Fig. 4a, as-prepared OFETs) up to 109 V (Fig. 4b, OFETs pre-treated by ozone treatment) in short time, indicating the role of organic n-type electrets in manipulating the charge transport inside C_8-BTBT film. Photo-induced electrons are transferred from donor (C_8-BTBT) to degraded acceptor (C_8-PTCDI), leading to charged acceptor with neat charge densities (Δn)[32],

$$\Delta n = \frac{V_{MW} \times C_{total}}{e} \tag{3}$$

where e is the element charge ($\sim 1.6 \times 10^{-19}$ C). The maximum value of V_{MW} is 109 V (Fig. 4b). Actually, the total areal capacitance C_{total} can be calculated by using $1/C_{total} = (1/C_{SiO2} + 1/C_{FPS})$, where 11.5 nF·cm^{-2} of C_{SiO2} denotes the specific capacitance of 300 nm SiO$_2$ and $C_{FPS} = \varepsilon_0 \cdot \varepsilon_{FPS}/d$. ε_0, the permittivity of vacuum, is $\sim 8.85 \times 10^{-12}$ F·m^{-1}. d, the thickness of FPS layer, is ~ 10.6 nm (Supplementary Fig. 7). ε_{FPS}, measured at room temperature and frequency of 1000 Hz, is 2.85[31]. For 10.6 nm FPS, C_{total} is calculated as 10.97 nF·cm^{-2}. Δn of 7.47×10^{12} cm^{-2}, calculated from Equation 1, is approaching or

even exceeding those of good insulator electrets. As has been pointed out above, most electrons were trapped in degraded C_8-PTCDI. Assuming that only one electron is transferred from C_8-BTBT to one degraded C_8-PTCDI molecule, the number of degraded C_8-PTCDI molecules are no more than 7.47×10^{12} cm^{-2}, which is $\approx 1/100$ of total molecules in 2 nm C_8-PTCDI film. As has been mentioned above, the energy levels between the as-prepared C_8-PTCDI film and degraded C_8-PTCDI film are almost unchanged, which can be explained by the low ratio of degraded C_8-PTCDI molecules and total molecules.

The relationship between memory performance and ozone treatment time is investigated (Supplementary Fig. 8). Memory on/off ratio and V_{MW} are both increased with the increase of ozone treatment time due to the fact that the number of organic n-type electrets is increased. That is, longer ozone treatment time is bound to generate more molecules of degraded organic n-type semiconductor, of which these degraded molecules are correlated with the organic n-type electrets. Once the number of organic n-type electrets is increased, I_{photo} is thus increased, and ΔV_{on} is well regulated in a wider range. Therefore, memory on/off ratio and V_{MW} are thus increased with ozone treatment. However, the OFETs performance is inevitably damaged for longer durations of ozone treatment[29], resulting in degradation of OFETs memory performance. Note that in erasing operation, the transfer curves are measured once light illumination is turned off, which is different from previous photoconductivity test.

To validate the role of organic n-type electrets in improving V_{MW}, C_8-BTBT-based

OFETs, without C_8-PTCDI, are fabricated. From programming state to erasing state, the as-prepared pure C_8-BTBT based OFETs show photoresponsive features, namely I_{ds} is increased under light illumination, which can be referred to the increase of hole concentrations. That is, once the OFETs are exposed to light illumination, electrons can be extracted out from semiconductor film under electric field, due to the weak binding between electron-hole pairs[33]. However, the transfer curves of erasing state are failed to be turned back to that of initial state, even the OFETs were pre-treated by ozone treatment (Supplementary Fig. 9), indicating organic n-type electrets are indeed critical. Interestingly, V_{MW} is increased after OFETs were pre-treated by ozone treatment, which can be attributed to the increase of film conductance, and exciton concentration is thus reduced.

The field-effect mobility and charge densities are one of the key factors of OFETs and OFETs memories, respectively, which is crucial in practical device applications. Here, the statistics of field-effect mobility and charge densities are investigated from over 30 papers (Fig. 4c), showing that most OFETs memories suffer from the relative lower field-effect mobility. For example, OFETs with configuration of MH(APy)-b-PS /pentacene are featured with high charge densities of 7.05×10^{12} cm^{-2}, of which the field-effect mobility is only 0.66 $cm^2 \cdot V^{-1} \cdot s^{-1}$ [34]. To improve field-effect mobility, without reduction in charge densities, C_{12}-BTBT/FPS based OFETs were both achieved with high field-effect mobility of 11.2 $cm^2 \cdot V^{-1} \cdot s^{-1}$ and high charge densities of 6.8×10^{12} cm^{-2} [31]. However, C_{12}-BTBT/FPS based OFETs suffer from long durations by applying

gate stress[31]. To address these issues, organic n-type electrets are added in C_8-

BTBT/FPS based OFETs, and high field-effect mobility of 13.3 $cm^2 \cdot V^{-1} \cdot s^{-1}$ and high

charge densities with 7.47×10^{12} cm^{-2} were both achieved within short time in this work.

The field-effect mobility in saturation regime can be calculated using the following

equation:

$$\mu = \frac{2L}{WC_i}(\frac{\partial \sqrt{I_{ds}}}{\partial V_{gs}})^2 \qquad (2)$$

where W and L is channel width and channel length, respectively. In addition to field-

effect mobility and charge densities, other crucial parameters are summarized in

Supplementary Table 1.

On the other hand, long-term memory stability is another key factor that

determines whether the devices can be practically used. The OFETs memories, with

configuration of degraded C_8-PTCDI/C_8-BTBT/FPS, show a good cycle repeatability

and environmental stability in erasing state. That is, the maximum absolute value of I_{ds}

is not decreased even after V_{gs} sweep for 100 times (Fig. 4d). When OFETs are exposed

in ambient for 4 weeks, the maximum absolute value of I_{ds} is reduced by only half (Fig.

4e). Meanwhile, memory on/off ratio is well kept over 10^6 for 10^4 s. By extending fitting

lines, memory on/off ratio is ~10 for over 10 years (Fig. 4f). All these measurements

were taken in ambient conditions with humidity of ~45 %.

To further validate the universality of organic n-type electrets in tuning charge

transport of p-type semiconductors, three strategies including insulator polymers that

can replace FPS, a different p-type conjugated polymer (PCDTPT) with C_8-PTCDI, and

C_8-BTBT with different degraded n-type semiconductors ($PC_{71}BM$, Br-NDI) are investigated as follows.

PS, as the alternative to FPS, is used to fabricate OFETs with configuration of C_8-PTCDI/C_8-BTBT/PS. After ozone treatment, V_{MW} is boosted from 8 V to 65 V (Supplementary Fig. 10), indicating that PS doesn't affect the role of organic n-type electrets in tuning charge transport of OFETs. As has been reported before, FPS is featured with more hole traps than that of PS[31], resulting in bigger negative shift of transfer curves after programming operation (V_{gs} = -100 V for 1 s). Therefore, V_{MW} of C_8-PTCDI/C_8-BTBT/FPS OFETs is larger. Because PS doesn't affect the role of organic n-type electrets, in the following investigation, PS is used to replace FPS. In addition to the replacement of insulator polymers, different organic n-type electrets were investigated in this work. OFETs, with configuration of both $PC_{71}BM$/C_8-BTBT/PS and Br-NDI/C_8-BTBT/PS, show the increase of V_{MW} (up to 60 V) after ozone treatment (Supplementary Fig. 11). Finally, the conjugated polymer of PCDTPT is used as a p-type semiconductor. The OFETs, with configuration of PCDTPT/C_8-PTCDI, demonstrate an increase of V_{MW} (up to 40 V) after heating at 120 $^\circ$C in ambient condition for one hour (Supplementary Fig. 12). In a word, organic n-type electrets are somehow universal for improving OFETs memories.

In addition to OFETs memories, organic n-type electrets also show their potential applications in light stimulated synaptic transistors, and several important neuronal/synaptic functions, such as excitatory postsynaptic current (EPSC), paired

pulse facilitation (PPF), short term memory (STM) and long term memory (LTM) are studied.

The recognition of pictures through human eyes is actually a process of information transfer, learning and memory, while the carriers of information are neurotransmitters (Fig. 5a). The neurotransmitters, via neurons, are eventually transmitted to visual cortex and STM or LTM is built in brains. Due to the neurons are connected by synapses, the transmission of information necessarily passes through synapse, resulting in the release of excitatory neurotransmitters in synaptic gap and EPSC is thus formed[28]. Although the principles of information processing in human brains are relatively poorly understood, the human brains, can process large amounts of information in parallel with high efficiency and low power consumption, show huge superiority compared to conventional computers based on von Neumann architecture[35]. Due to the challenge of "von Neumann bottleneck", bionic study of human brain using transistors attracts a wide range of research in academic community[36]. However, light stimulated synaptic transistors using n-type electrets is rarely reported.

As is shown in Fig. 5b, EPSC is low, while it is rapidly increased by light spike with pulse width (ΔT) of 1 s. When the light illumination is removed, EPSC is decreased and eventually stabilized, of which the stabilized EPSC is still larger than that of the initial state. This phenomenon becomes more pronounced when two consecutive light pulses with pulse width (ΔT_1) of 1 s and spike time interval (ΔT_2) of 1 s are applied (Fig. 5c). That is, once two consecutive light pulses are applied and then are removed,

the stabilized EPSC is increased from 11 nA to 28 nA, which is STM. STM is bound to be appeared more frequently by more successive light pulses, and eventually STM leads to LTM.[37] Therefore, after light pulses is applied for hundreds of times, the steady-state EPSC becomes larger and larger (Fig. 5d). This is analogous to human learning and memory. For example, when an ordinary child tries to recite a new verse, short term synaptic plasticity is built in his mind, however, this memory is not solid and it is hard to recite fluently. After learning to recite for many times, synaptic weights about the verse are increased and long term synaptic plasticity is built. Once LTM is formed, the verse is engraved in a specific area of nervous system.

In terms of memory effectiveness, the number of times to study is important, but the frequency of study is equally crucial, because longer time intervals can lead to STM or even forgetting[38]. PPF, as a typical form of short term synaptic plasticity, is the ratio of the maximum EPSC value from the second spike to that of the first spike[28], which is related to ΔT_2 and can be fitted by a double exponential function:

$$PPF = 1 + A_1 \cdot e^{\frac{-\Delta T_2}{\tau_1}} + A_2 \cdot e^{\frac{-\Delta T_2}{\tau_2}} \qquad (3)$$

where A_1 and A_2 represents the value of initial fast and slow phase facilitation, respectively. The fitting result of $\tau_1 = 66$ ms and $\tau_2 = 320$ ms is obtained, which is equivalent to those of biological synapses (Fig. 5e). Long term synaptic plasticity is fundamental for LTM, while short term synaptic plasticity can lead to long term synaptic plasticity through repeated rehearsals[39-40]. In summary, the frequency of study plays a key role in LTM.

To further investigate learning ability based on synaptic behavior of light stimulated synaptic transistors, the Modified National Institute of Standards and Technology (MNIST) database is thus used[41]. As is known, learning ability is actually the iterative repetition by assigning weights and retraining[28]. In this work, Fig. 5f demonstrates total 100 channel conductance values, as the basis for increasing or decreasing the weights in artificial neural networks (Fig. 5g). The equations for conductance (G) and number of pulses (P) are[35]:

$$G_\mathrm{P} = \frac{(G_\mathrm{max} - G_\mathrm{min}) \cdot (1 - e^{\frac{-P}{A}})}{1 - e^{\frac{-P_\mathrm{max}}{A}}} + G_\mathrm{min} \tag{4}$$

$$G_\mathrm{D} = \frac{(G_\mathrm{min} - G_\mathrm{max}) \cdot (1 - e^{\frac{P - P_\mathrm{max}}{A}})}{1 - e^{\frac{-P_\mathrm{max}}{A}}} + G_\mathrm{max} \tag{5}$$

where G_max, G_min and P_max are taken directly from experimental data, which represent the maximum conductance value, the minimum conductance value and the maximum number of pulses, respectively. G_P and G_D denote conductivity enhancement and conductivity decrease, respectively. A is related to nonlinearity (NL) that controls weights update, and their relationship can be referred in previous report[37]. The weight updating method is available in previous reports[42-43].

In this work, NL is low under illumination conditions ($NL_\mathrm{P} = 0.05$) because one photon induces an electron into n-type electrets and simultaneously induces a hole in p-type semiconductors, resulting in an approximately linear enhancement of conductance under light illumination. When positive V_gs is applied, the gate electric

field causes holes in p-type semiconductors to inject into the n-type electrets, and these holes are recombined with the electrons previously stored in n-type electrets, resulting in those electrons in n-type electrets are decreased exponentially. Therefore, the conductance is rapidly decreased in the first few pulses. As the recombination of electrons-holes is on-going, the electron concentrations in n-type electrets are decreased, making the recombination relatively slower, and the decrease of conductance is relatively slower in the last few pulses. Therefore, the nonlinearity under positive V_{gs} is larger, and $NL_D = 2.44$.

As shown in Fig. 5h, the overall recognition accuracy of artificial neural network grows fast at first and gradually saturates with the increase of training epochs. When the number of training epochs reaches 200, the overall recognition rate is 65%, which is comparable to previously reports of other systems[42,44]. To quantitatively illustrate the performance of artificial neural network, we calculated recognition rates for 0 to 9 digits, as shown in Fig. 5i. The recognition rates of "1" (the character with the highest recognition rate) and "8" (the character with the lowest recognition rate) are 0.93 and 0.08, respectively.

CONCLUSION

In conclusion, we propose a class of electrets, namely organic n-type electrets, made by oxygen-degraded n-type organic semiconductors. In this work, n-type semiconductors interact with oxygen species including air, ozone or oxygen plasma for in-situ degradation. After degradation, the electron mobility of n-type semiconductors is rapidly decreased, warranting an insulating characteristic of the oxygen-degraded

semiconductor for organic n-type electrets. Afterwards, photo-induced electrons are transferred from p-type semiconductor to the degraded n-type semiconductor, and the charged degraded n-type semiconductors are n-type electrets. As compared with conventional insulator electrets, organic n-type electrets are featured with appropriate electron affinity, warranting charge transfer under light illumination and good charge trap (storage) ability. The sheet charge densities of such n-type electret films, as high as 7.47×10^{12} cm^{-2}, is used to provide steady built-in electric field to significantly improve the performance of OFET. OFETs made of C$_8$-BTBT in combination with n-type electret based on C$_8$-PTCDI, show field-effect mobility 13.3 cm$^2 \cdot$V$^{-1} \cdot$s^{-1}, along with a memory window over 100 V, a memory on/off ratio 10^6 and a stable retention life time over one month in ambient air. Afterwards, OFETs with organic n-type electrets are employed in artificial synapse, and the recognition rate of brain-inspired neuromorphic computing is 65%.

METHODS

Device Preparation: Si/SiO$_2$ substrate was cleaned by deionized water, acetone and isopropanol in sequence, and then dried using nitrogen gas flow. Afterwards, FPS (laboratory synthesized) and PS (M_w = 2000 kDa, PDI = 1.3, purchased from Sigma-Aldrich), dissolved in o-dichlorobenzene with a concentration of 5 mg·ml^{-1}, were spin-coated on bare Si/SiO$_2$ substrate for 120 s at 2000 rpm and then annealed at 130 °C for 30 min in ambient condition, respectively. Then, C$_8$-BTBT (purchased from J&K Scientific), C$_8$-PTCDI (purchased from Ogantec Ltd.), PC$_{71}$BM (purchased from Ogantec Ltd.), and Br-NDI (laboratory synthesized), without any other treatment, were

deposited in sequence by vacuum thermal evaporation ($< 10^{-4}$ Pa) with ratio of 0.1~0.2 Å/s. For PCDTPT (purchased from 1-Material), PCDTPT:PS = 5:95 blend solutions (o-dichlorobenzene as solvent) were spin-coated (2000 rpm for 120 s) on trichloro(phenyl)silane (purchased from Sigma-Aldrich)-modified Si/SiO$_2$ substrate. Finally, 50 nm gold source and drain electrodes were deposited through a shadow mask with channel length of 0.3 mm and width of 3 mm.

OFETs characterization: The OFETs characterization was performed using an Agilent Keysight B2900A Quick IV measurement system at ambient conditions.

Oxygen Plasma/Ozone Treatment and light illumination: The oxygen plasma treatment process was applied using FEMTO from Electronic Diener Plasma-Surface-Technology (13.56 MHz) with chamber pressure of 30 or 150 Pa. The ozone treatment was performed in atmospheric pressure (PSD UV4, NOVAS-CAN Inc.). For light source, portable LUYOR-3405 with adjustable light intensity was used.

Film morphology and spectroscopy characterizations: Contact mode atomic force microscopy pictures with scaling size of 10×10 μm^2 were obtained using Asylum Research Cypher. UV-vis and infrared absorbance of thin film were carried out by PerkinElmer Lambda950 UV-VIS-NIR Spectrometer and Thermo NICOLET 6700 FT-IR, respectively. Samples were prepared on quartz glass substrate and CaF$_2$ substrate for UV-vis and infrared absorbance, respectively.
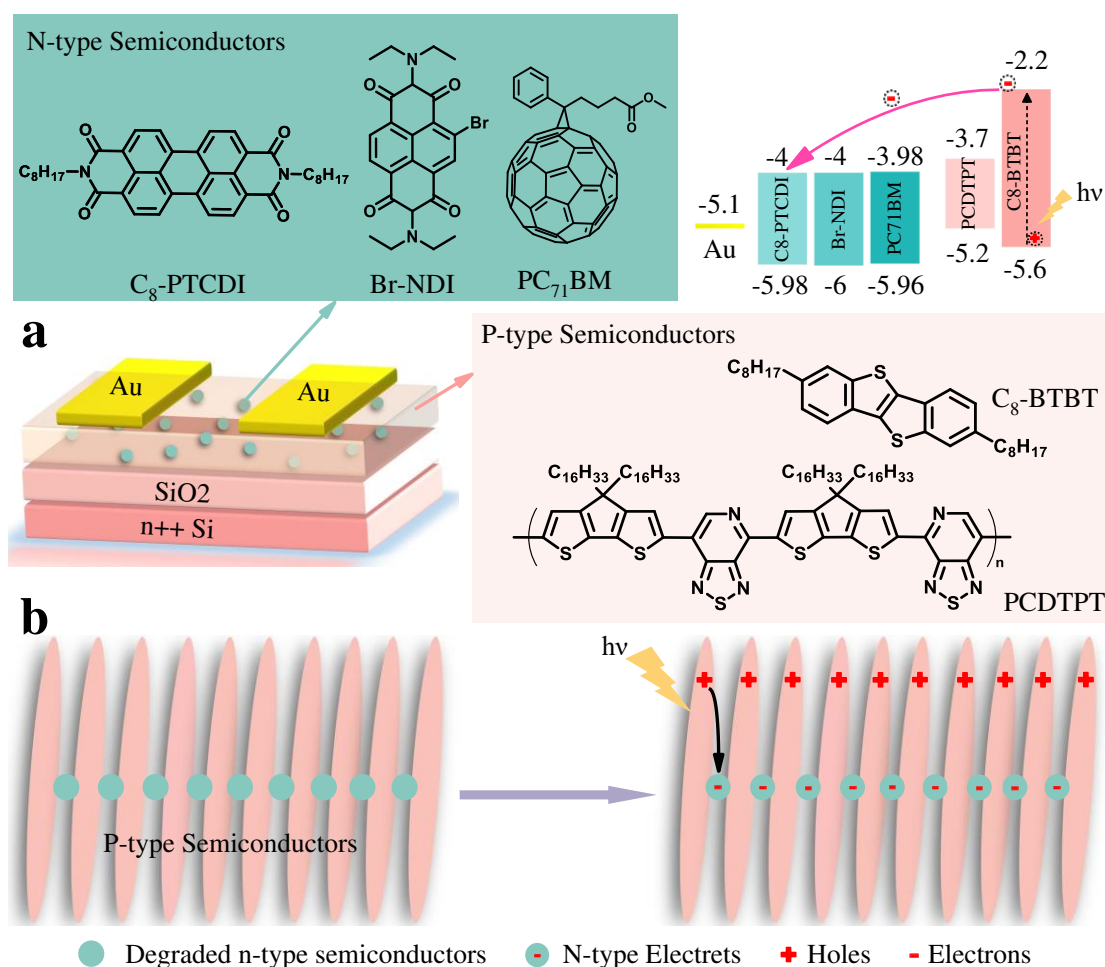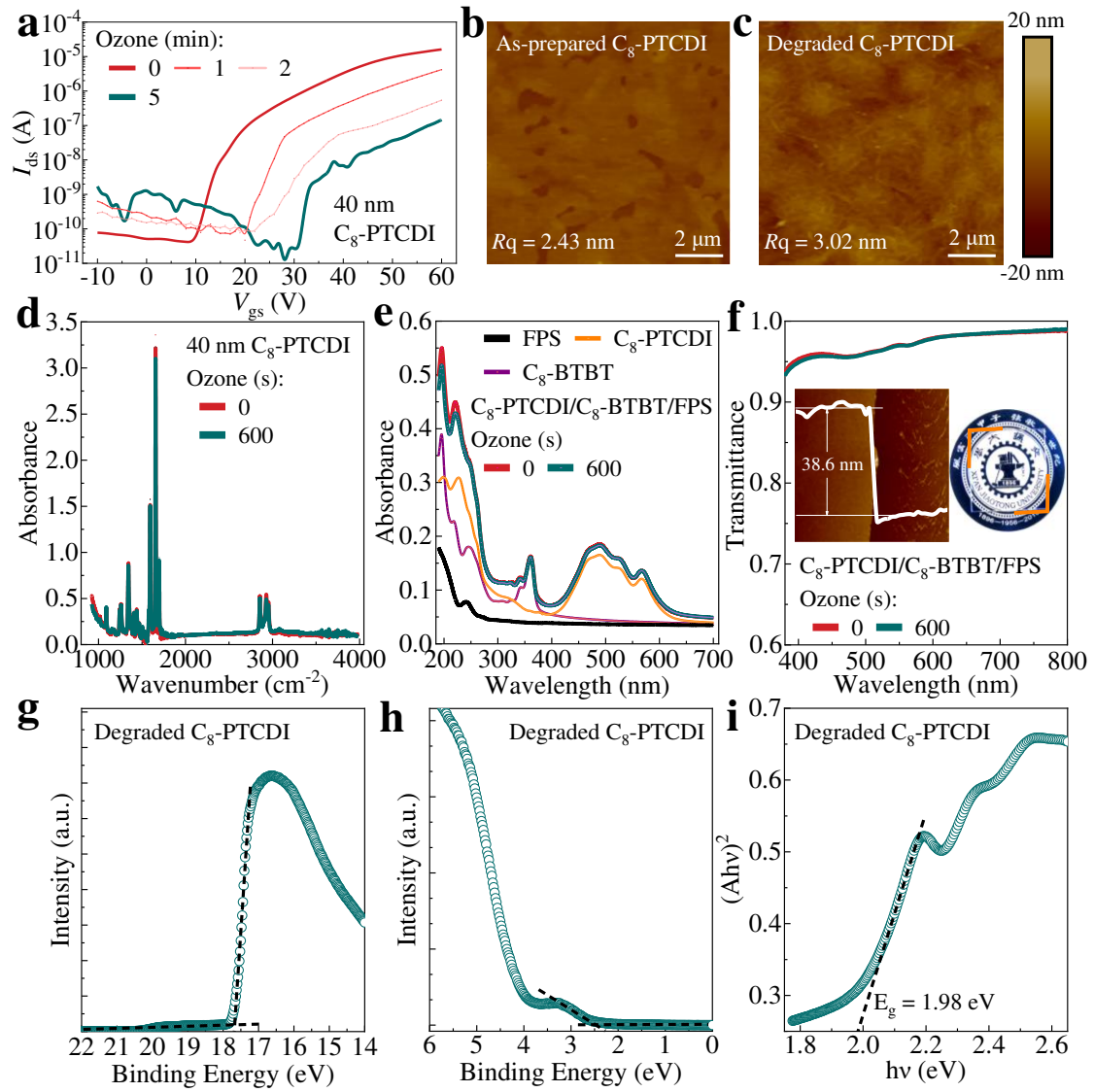
ASSOCIATED CONTENT
Supporting Information

The Supporting Information is available free of charge.

Notes

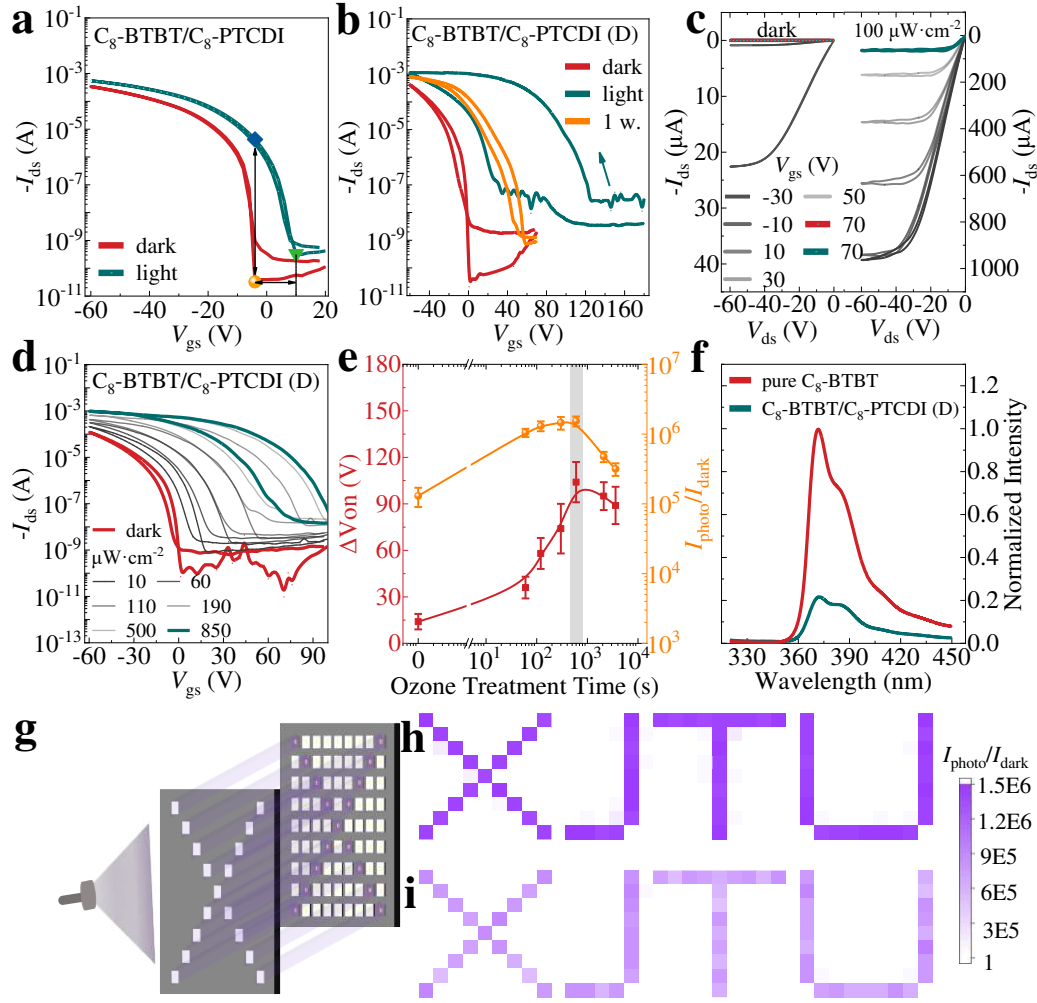The authors declare no competing financial interest.

Fig. 1 Materials and devices investigated in this work. a The molecular structures, energy levels of materials and device configuration. **b** The mechanism of n-type electrets for tuning the charge concentrations in p-type semiconductors. First, the n-type electret is generated upon exposing n-type semiconductors to oxygen species, which induces the material degradation. Then, the n-type electrets, carrying quasi-permanent neat charges, is obtained under light illumination in the n/p configuration: the photo-induced electron-hole pairs are split at the interface of n/p heterojunction, subsequently the electrons are transferred into and stably trapped in the n-type electrets (degraded n-type semiconductors). Finally, the built-in electric field, supplied by the n-type electrets, is used to manipulate the charge transport inside p-type semiconductors for OFET applications.
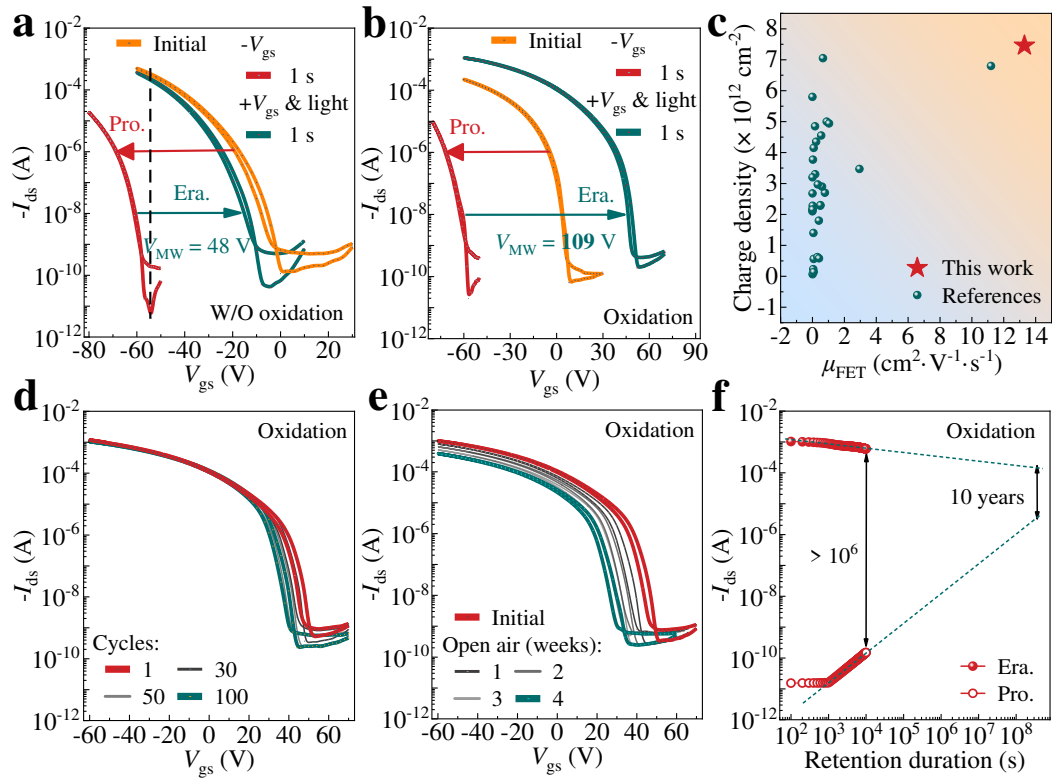
Fig. 2 Characterizations of oxidation-induced degradation of C$_8$-PTCDI thin films. a The transfer curves (V_{ds} = 60 V) of C$_8$-PTCDI-based OFETs by ozone treatment. **b-c** Atomic Force Microscopy (AFM) height images of the films (scanning sizes 10 × 10 μm^2) after ozone treatment for **b** 0 s and **c** 600 s. **d** Infrared absorbance spectra of the films without and with ozone treatment for 600 s. **e** UV-vis absorbance spectra of FPS, C$_8$-PTCDI, C$_8$-BTBT and C$_8$-PTCDI/C$_8$-BTBT/FPS configuration with and without ozone treatment for 600 s. **f** Optical transmittance spectra of the C$_8$-PTCDI/C$_8$-BTBT/FPS configuration without and with ozone treatment. Inset photograph shows an excellent optically transparency in visible light. **g-h** Ultraviolet photoelectron spectra of C$_8$-PTCDI film with ozone treatment for 600 s: **g** the secondary edge region and **h** the HOMO region. **i** The optical gap. The thickness of C$_8$-PTCDI thin films is 40 nm.
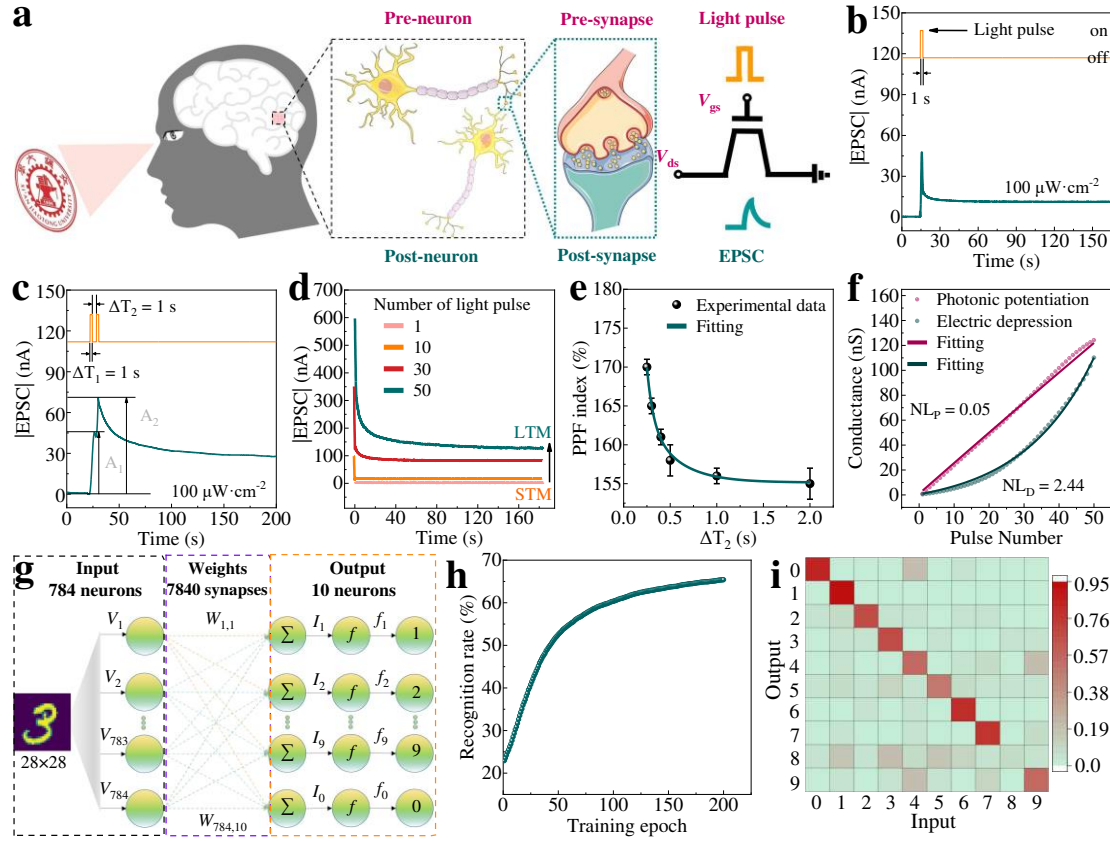
Fig. 3 The photo-response of C₈-BTBT-based OFETs with C₈-PTCDI. a-b In-situ transfer curves by ozone treatment for **a** 0 s and **b** 600 s in the dark and under light intensity of 1 mW·cm⁻², respectively. During the sweep of V_{gs}, the device was under light illumination. The abbreviation "1 w." denotes that the OFETs were placed in the open air with relative humidity 45% for 1 week after light illumination for 5 s. The abbreviation "C₈-PTCDI (D)" denote the C₈-PTCDI molecules were partially degraded by oxygen species, showing a degraded electrical performance. **c** Output curves of the OFETs in the dark and under fixed light intensity. **d** Transfer curves of the OFETs under different light intensities. **e** The dependence of ΔV_{on} and I_{photo}/I_{dark} ratio on the ozone treatment time. **f** Fluorescence spectra of pure C₈-BTBT film and C₈-PTCDI/C₈-BTBT (D) film excited at wavelength 365 nm. **g** The schematic diagram of the erasing process with the light wavelength of 365 nm through the hollowed plate mask with a "XJTU" pattern. The recorded light information of I_{photo}/I_{dark} ratio with "XJTU" pattern: **h** as-prepared, and **i** OFETs stored in open air with relative humidity 45% for 1 week. The OFETs were measured at V_{ds} = -60 V. The thicknesses of C₈-BTBT and C₈-PTCDI thin films are 40 nm and 2 nm, respectively.

31

**Fig. 4 The role of degraded C₈-PTCDI film as the organic n-type electrets for OFETs memories. a-
b** Transfer curves of OFETs based on 40 nm C₈-BTBT with 2 nm C₈-PTCDI after programming (V_{gs} = -
100 V for 1 s) and erasing (simultaneously applying V_{gs} = +100 V and light illumination with 1 mW·cm⁻
² for 1 s) processes. "Pro." and "Era." denote programming and erasing, respectively. The device in **b**
was pre-treated by ozone for 600 s to obtain degraded C₈-PTCDI. **c** The statistics of properties of electret-
containing OFETs in term of charge densities of electret and field-effect mobilities. Detailed comparisons
and references are provided in Supplementary Table 1. **d-e** Cycle repeatability for **d** and environmental
stability for **e** after erasing. **f** Retention life time of organic memory device. According to **b**, the reading
process was carried out at V_{on}. It is noted that the OFETs were measured at V_{ds} = -60 V.

Fig. 5 Emulation of synaptic functions by the C$_8$-BTBT/C$_8$-PTCDI (D) artificial synaptic OFETs.
a Scheme of a biological synapse and the C$_8$-BTBT/C$_8$-PTCDI (D) artificial synaptic OFETs. The skill of picture recognition by the human eye involves transmitting picture information through the retina to the visual cortex. Human body's mastery of skills is related to learning. Synapses connect neurons in the visual cortex of brain to each other, thus forming a neural network that can control the release of skills. **b** EPSC plot of the C$_8$-BTBT/C$_8$-PTCDI (D) artificial synaptic OFETs triggered by light spike (pulse width (ΔT): 1 s). **c** EPSC plot of the C$_8$-BTBT/C$_8$-PTCDI (D) artificial synaptic OFETs triggered by light spike (pulse width (ΔT_1): 1 s; spike time interval (ΔT_2): 1 s). **d** Evolution of EPSC after stimulation by various numbers of light pulses. **e** Plots of extracted PPF index (A$_2$/A$_1$) versus spike time interval (ΔT_2). A$_1$ and A$_2$ are the first and second EPSC peaks, respectively. The solid line is the fitted curve using double exponential function. **f** Schematic diagram of the applied photonic/electrical pulse sequence used to obtain the 50 weight states of synaptic devices. **g** Schematic diagram of an artificial neural network based on a single layer perceptron with 784 input neurons and 10 output neurons fully connected through 7840 synaptic weights. **h** Training function for the average recognition rate for 100 weight states, based on a MNIST test set of over 10,000 numbers from 0 to 9 in total. **i** Recognition capability of the artificial neural network. The diagonal of the matrix represents the recognition rate of 10 digits from 0-9, and the rest of the matrix represents the error rate. The artificial synaptic OFETs were measured at V_{ds} = -5 V.

REFERENCES

1. Wen, X., Li, D., Tan, K., et al. Flexoelectret: An electret with a tunable flexoelectriclike response. *Phys. Rev. Lett.* **122**, 148001 (2019).

2. Zhao, J., Wei, Z., Zhang, Q., et al. Static and dynamic piezopotential modulation in piezo-electret gated mos2 field-effect transistor. *ACS Nano* **13**, 582-590 (2019).

3. Li, Z. B., Li, H. Y., Fan, Y. J., et al. Small-sized, lightweight, and flexible triboelectric nanogenerator enhanced by ptfe/pdms nanocomposite electret. *ACS Appl. Mater. Interfaces* **11**, 20370-20377 (2019).

4. Mendel, N., Wu, H. & Mugele, F. Electrowetting-assisted generation of ultrastable high charge densities in composite silicon oxide–fluoropolymer electret samples for electric nanogenerators. *Adv. Funct. Mater.* **31**, 2007872 (2021).

5. Feng, Y., Zhou, Z. L., Fu, D. X., et al. Velocity-amplified monostable dual-charged electret dome energy harvester using low-speed finger tapping. *Appl. Phys. Lett.* **116**, 063905 (2020).

6. Gerlach, A., Liebler, M., Sessler, G. M., et al. Comparative analysis of isothermal decay of the surface potential of fluoroethylenepropylene electrets and of the sensitivity of electret microphones at elevated temperature. *AIP Adv.* **10**, 095313 (2020).

7. Liu, H., Zhang, S. C., Liu, L. F., et al. High-performance pm0.3 air filters using self-polarized electret nanofiber/nets. *Adv. Funct. Mater.* **30**, 1909554 (2020).

8. Lee, Y. R., Trung, T. Q., Hwang, B. U., et al. A flexible artificial intrinsic-synaptic tactile sensory organ. *Nat. Commun.* **11**, 2753 (2020).

9. Li, D., Zhu, Y., Wei, P., et al. Polymer electret improves the performance of the oxygen-doped organic field-effect transistors. *IEEE Electron Device Lett.* **41**, 1665-1668 (2020).

10. She, X. J., Gustafsson, D. & Sirringhaus, H. A vertical organic transistor architecture for fast nonvolatile memory. *Adv. Mater.* **29**, 1604769 (2017).

11. Hu, Y., Wei, P., Wang, X., et al. Giant transconductance of organic field-effect transistors in compensation electric fields. *Phys. Rew. Appl.* **10**, 054024 (2018).

12. Lu, G., Koch, N. & Neher, D. In-situ tuning threshold voltage of field-effect transistors based on blends of poly (3-hexylthiophene) with an insulator electret. *Appl. Phys. Lett.* **107**, 063301 (2015).

13. Baeg, K. J., Noh, Y. Y., Ghim, J., et al. Organic non-volatile memory based on pentacene field-effect transistors using a polymeric gate electret. *Adv. Mater.* **18**, 3179-3183 (2006).

14. Li, D., Li, S., Lu, W., et al. Rapidly measuring charge carrier mobility of organic semiconductor films upon a point-contact four-probes method. *IEEE J. Electron Devices Soc.* **7**, 303-308 (2018).

15. Jeong, Y. J., Yun, D. J., Noh, S. H., et al. Surface modification of cdse quantum-dot floating gates for advancing light-erasable organic field-effect transistor memories. *ACS Nano* **12**, 7701-7709 (2018).

16. Lan, S., Zhong, J., Li, E., et al. High-performance nonvolatile organic photoelectronic transistor memory based on bulk heterojunction structure. *ACS Appl. Mater. Interfaces* **12**, 31716-31724 (2020).

17. Wang, C., Dong, H., Jiang, L., et al. Organic semiconductor crystals. *Chem. Soc. Rev.* **47**, 422-500 (2018).

18. Ren, Y., Zhu, Y., Li, D., et al. Light-assisted charge injection and depletion of insulator electrets for organic field-effect transistors. *J. Mater. Chem. C* **7**, 12862-12868 (2019).

19. Zhang, G., Lee, S., Gutiérrez-Meza, E., et al. Robust and stretchable polymer semiconducting networks: From film microstructure to macroscopic device performance. *Chem. Mater.* **31**, 6530-6539 (2019).

20. Patel, J. B., Tiwana, P., Seidler, N., et al. Effect of ultraviolet radiation on organic photovoltaic materials and devices. *ACS Appl. Mater. Interfaces* **11**, 21543-21551 (2019).

21. Yang, F. S., Li, M., Lee, M. P., et al. Oxidation-boosted charge trapping in ultra-sensitive van der waals materials for artificial synaptic features. *Nat. Commun.* **11**, 2972 (2020).

22. Wei, P., Li, X., Wang, L., et al. Vertical-resolved composition and aggregation gradient of conjugated-polymer@insulator-matrix for transistors and memory. *Adv. Electron. Mater.* **6**, 1901156 (2020).

23. Zheng, L., Zhu, T., Xu, W., et al. Solution-processed broadband polymer photodetectors with a spectral response of up to 2.5 μm by a low bandgap donor–acceptor conjugated copolymer. *J. Mater. Chem. C* **6**, 3634-3641 (2018).

24. Tauc, J., Grigorovici, R. & Vancu, A. Optical properties and electronic structure of amorphous germanium. *Phys. Status Solidi* **15**, 627-637 (1966).

25. Park, S., Lee, B., Bae, B., et al. Ambipolar thin-film transistors based on organic semiconductor blend. *Synth. Metals* **253**, 40-47 (2019).

26. Zhang, L., Zhong, X., Pavlica, E., et al. A nanomesh scaffold for supramolecular nanowire optoelectronic devices. *Nat. Nanotechnol.* **11**, 900-906 (2016).

27. Za'aba, N. K. & Taylor, D. M. Photo-induced effects in organic thin film transistors based on dinaphtho [2,3-b:2′,3′-f] thieno[3,2-b′] thiophene (dntt). *Org. Electron.* **65**, 39-48 (2019).

28. Yang, B., Lu, Y., Jiang, D., et al. Bioinspired multifunctional organic transistors based on natural chlorophyll/organic semiconductors. *Adv. Mater.* **32**, 2001227 (2020).

29. Qiu, Y., Wei, P., Wang, Z., et al. Manipulating doping of organic semiconductors by reactive oxygen for field-effect transistors. *Phys. Status Solidi RRL* **12**, 1800297 (2018).

30. Wang, Y., Lv, Z., Chen, J., et al. Photonic synapses based on inorganic perovskite quantum dots for neuromorphic computing. *Adv. Mater.* **30**, 1802883 (2018).

31. Zhu, Y., Fan, Y., Li, S., et al. Soluble poly(4-fluorostyrene): A high-performance dielectric electret for organic transistors and memories. *Mater. Horiz.* **7**, 1861-1871 (2020).

32. Podzorov, V. & Gershenson, M. E. Photoinduced charge transfer across the interface between organic molecular crystals and polymers. *Phys. Rev. Lett.* **95**, 016602 (2005).

33. Yuan, Y. & Huang, J. Ultrahigh gain, low noise, ultraviolet photodetectors with highly aligned organic crystals. *Adv. Opt. Mater.* **4**, 264-270 (2016).

34. Yu-Cheng, C., Issei, O., Sami, H., et al. High-performance nonvolatile transistor memories of pentacene using the green electrets of sugar-based block copolymers and their supramolecules. *Adv. Funct. Mater.* **24**, 4240-4249 (2014).

35. Chen, P.-Y., Peng, X. & Yu, S. Neurosim: A circuit-level macro model for benchmarking neuro-inspired architectures in online learning. *IEEE Trans. Comput.-Aided Design Integr. Circuits Syst.* **37**, 3067-3080 (2018).

36. Liu, Z., Tang, J., Gao, B., et al. Neural signal analysis with memristor arrays towards high-efficiency brain-machine interfaces. *Nat. Commun.* **11**, 4234 (2020).

37. Yu, R., Li, E., Wu, X., et al. Electret-based organic synaptic transistor for neuromorphic computing. *ACS Appl. Mater. Interfaces* **12**, 15446-15455 (2020).

38. Ahmed, T., Kuriakose, S., Mayes, E. L. H., et al. Optically stimulated artificial synapse based on layered black phosphorus. *Small* **15**, e1900966 (2019).

39. Ohno, T., Hasegawa, T., Tsuruoka, T., et al. Short-term plasticity and long-term potentiation mimicked in single inorganic synapses. *Nat. Mater.* **10**, 591-595 (2011).

40. Abbott, L. F., Regehr, W. G. Synaptic computation. *Nature*, **431**, 796-803 (2004).

41. Lv, Z., Chen, M., Qian, F., et al. Mimicking neuroplasticity in a hybrid biopolymer transistor by dual modes modulation. *Adv. Funct. Mater.* **29**, 1902374 (2019).

42. Sun, J., Oh, S., Choi, Y., et al. Optoelectronic synapse based on igzo-alkylated graphene oxide hybrid structure. *Adv. Funct. Mater.* **28**, 1804397 (2018).

43. Seo, S., Jo, S. H., Kim, S., et al. Artificial optic-neural synapse for colored and color-mixed pattern recognition. *Nat. Commun.* **9**, 5106 (2018).

44. Kim, S., Choi, B., Lim, M., et al. Pattern recognition using carbon nanotube synaptic transistors with an adjustable weight update protocol. *ACS Nano* **11**, 2814-2822 (2017).
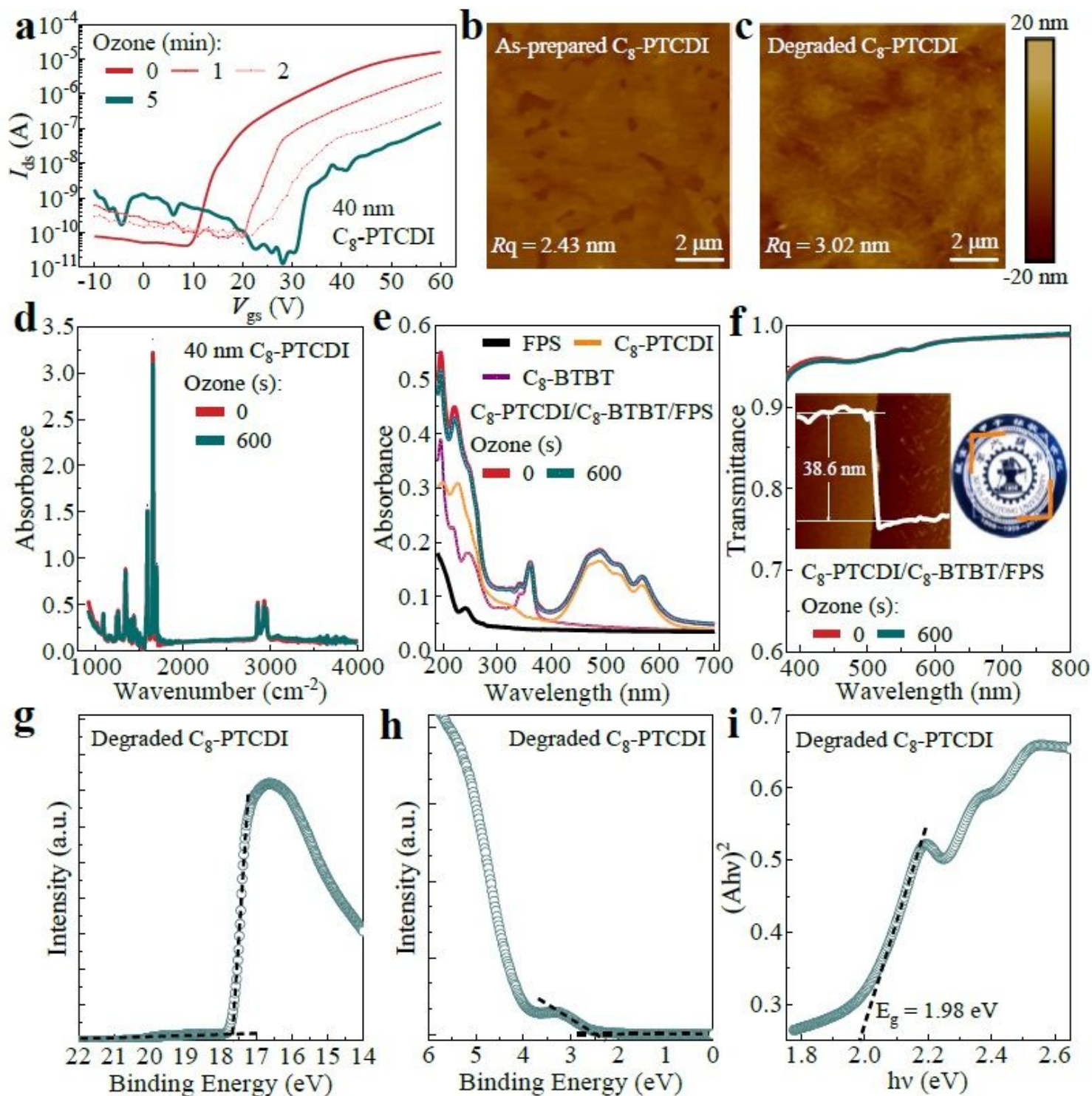
Figures
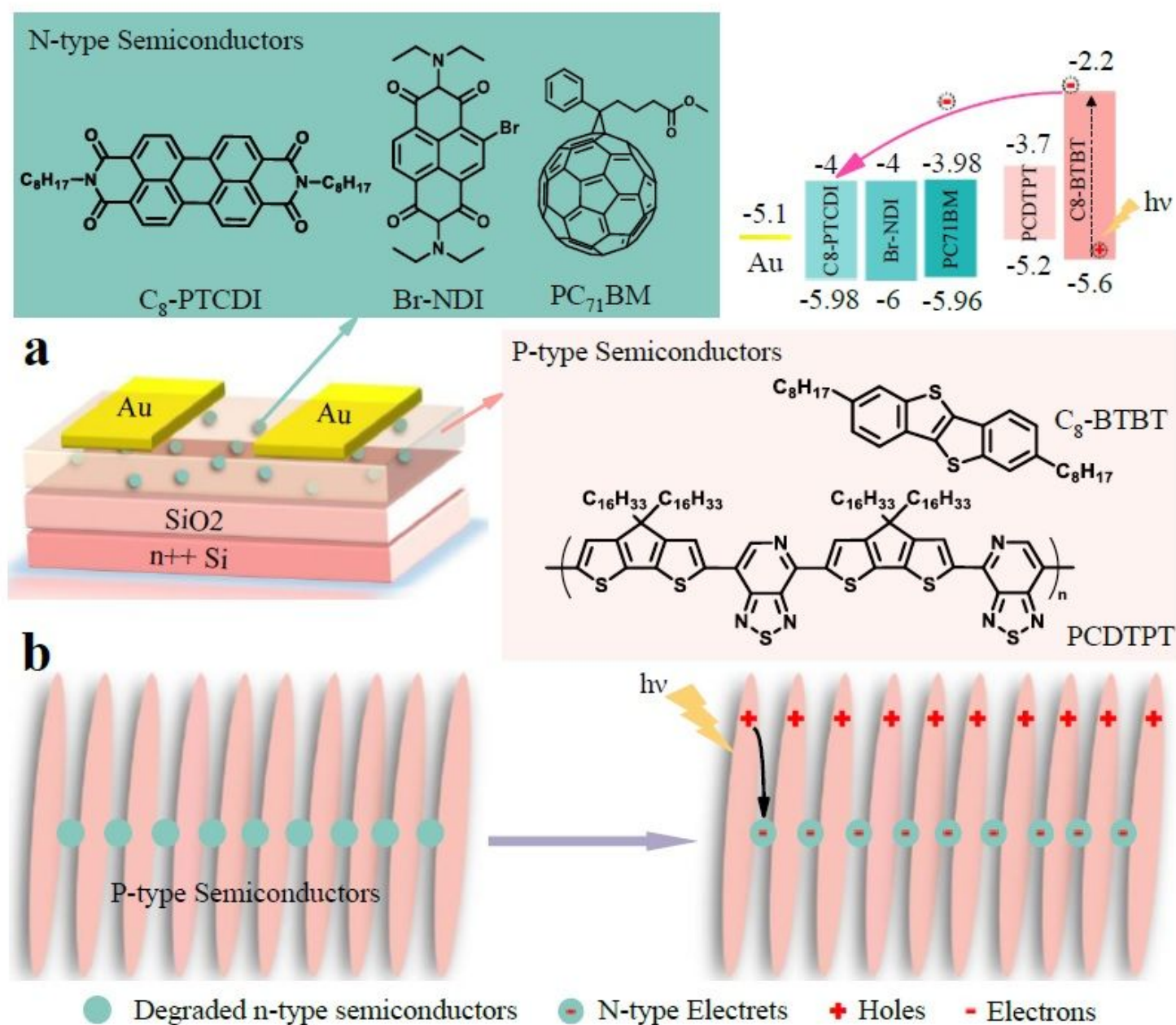
Figure 1

Materials and devices investigated in this work. a The molecular structures, energy levels of materials and device configuration. b The mechanism of n-type electrets for tuning the charge concentrations in p-type semiconductors. First, the n-type electret is generated upon exposing n-type semiconductors to oxygen species, which induces the material degradation. Then, the n-type electrets, carrying quasi-permanent neat charges, is obtained under light illumination in the n/p configuration: the photo-induced electron-hole pairs are split at the interface of n/p heterojunction, subsequently the electrons are transferred into and stably trapped in the n-type electrets (degraded n-type semiconductors). Finally, the

built-in electric field, supplied by the n-type electrets, is used to manipulate the charge transport inside p-type semiconductors for OFET applications.

Figure 2

Characterizations of oxidation-induced degradation of C8-PTCDI thin films. a The transfer curves (Vds = 60 V) of C8-PTCDI-based OFETs by ozone treatment. b-c Atomic Force Microscopy (AFM) height images of the films (scanning sizes 10 × 10 μm2) after ozone treatment for b 0 s and c 600 s. d Infrared

absorbance spectra of the films without and with ozone treatment for 600 s. e UV-vis absorbance spectra of FPS, C8-PTCDI, C8-BTBT and C8-PTCDI/C8-BTBT/FPS configuration with and without ozone treatment for 600 s. f Optical transmittance spectra of the C8-PTCDI/C8-BTBT/FPS configuration without and with ozone treatment. Inset photograph shows an excellent optically transparency in visible light. g-h Ultraviolet photoelectron spectra of C8-PTCDI film with ozone treatment for 600 s: g the secondary edge region and h the HOMO region. i The optical gap. The thickness of C8-PTCDI thin films is 40 nm.
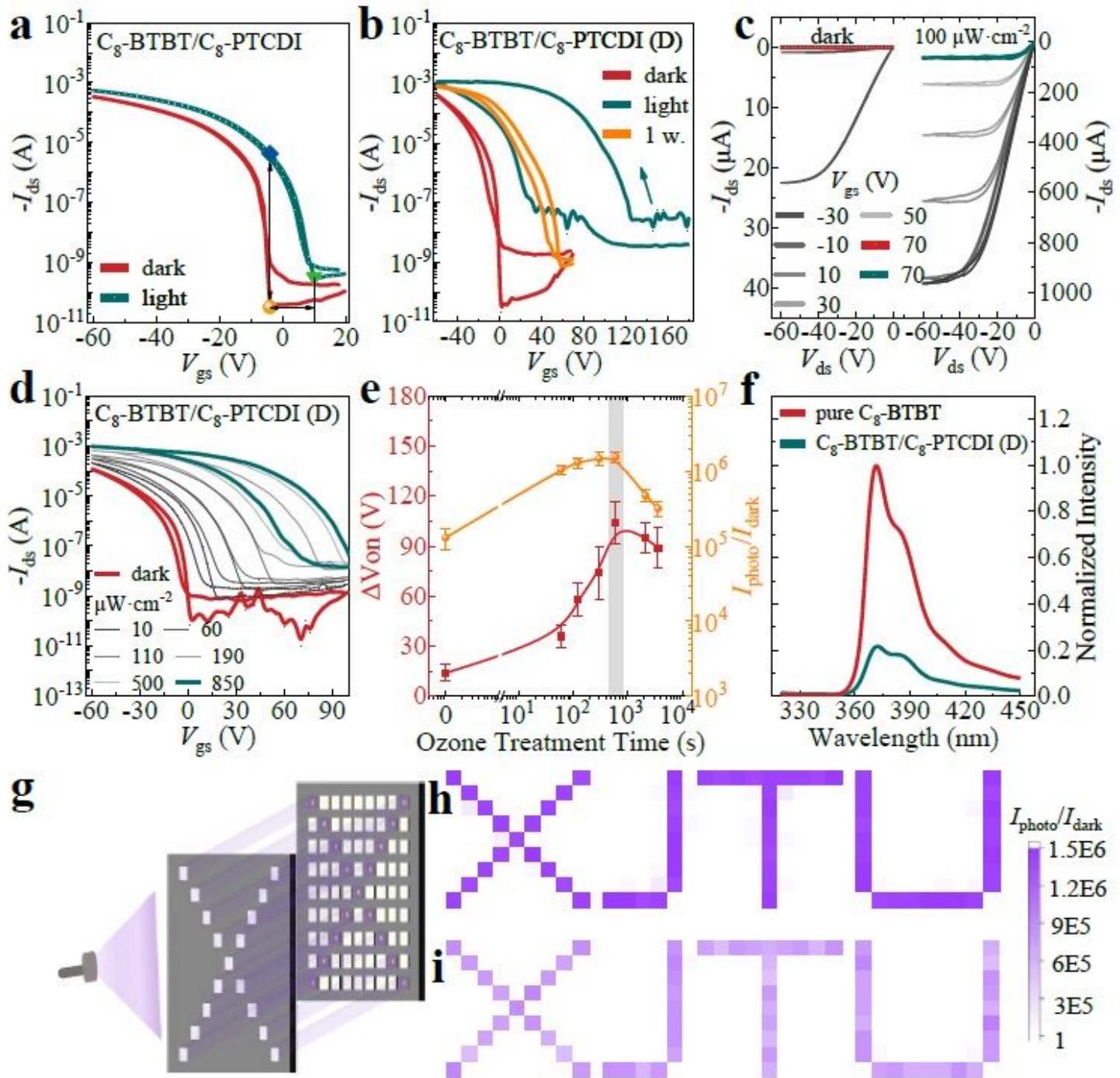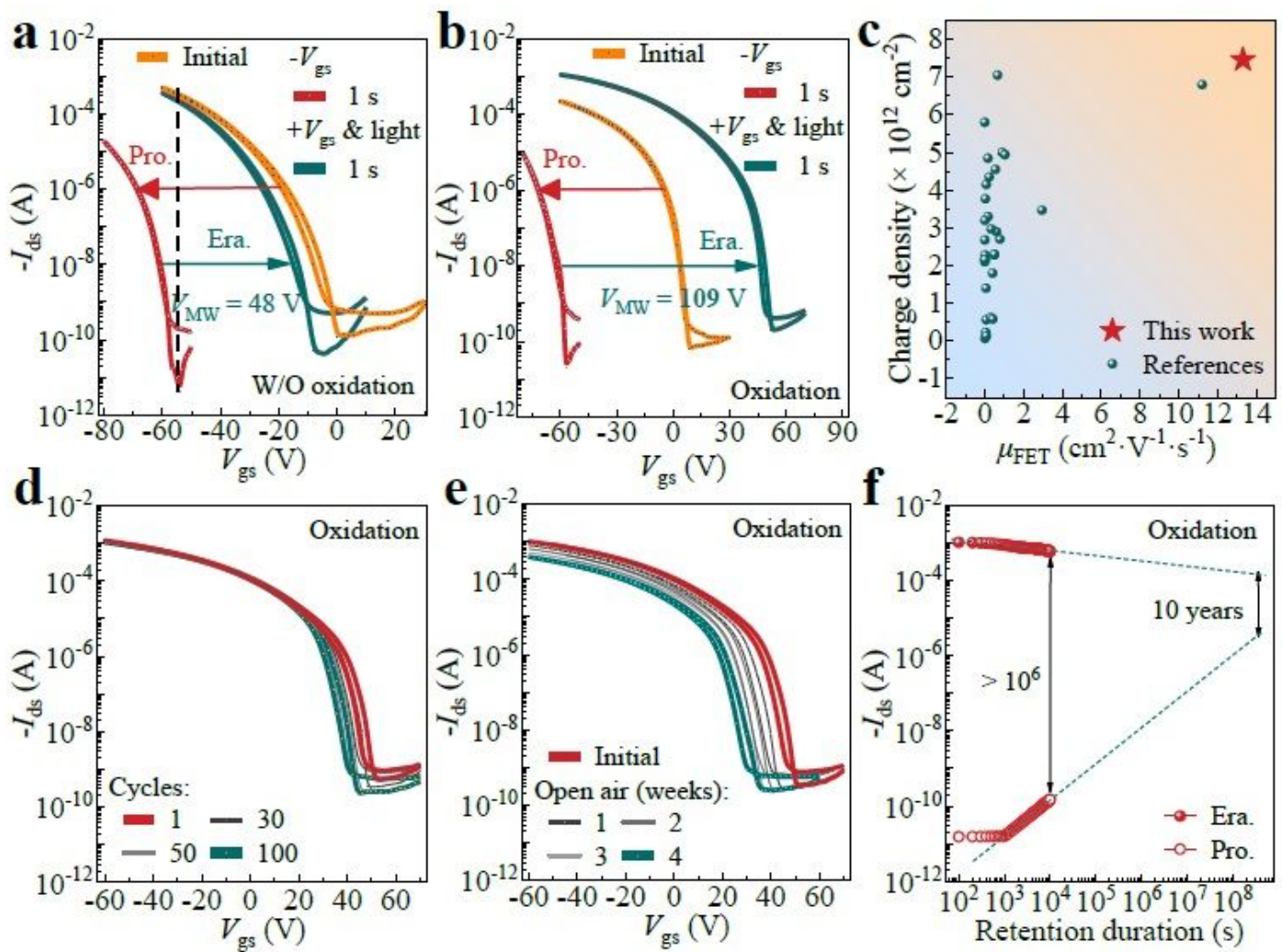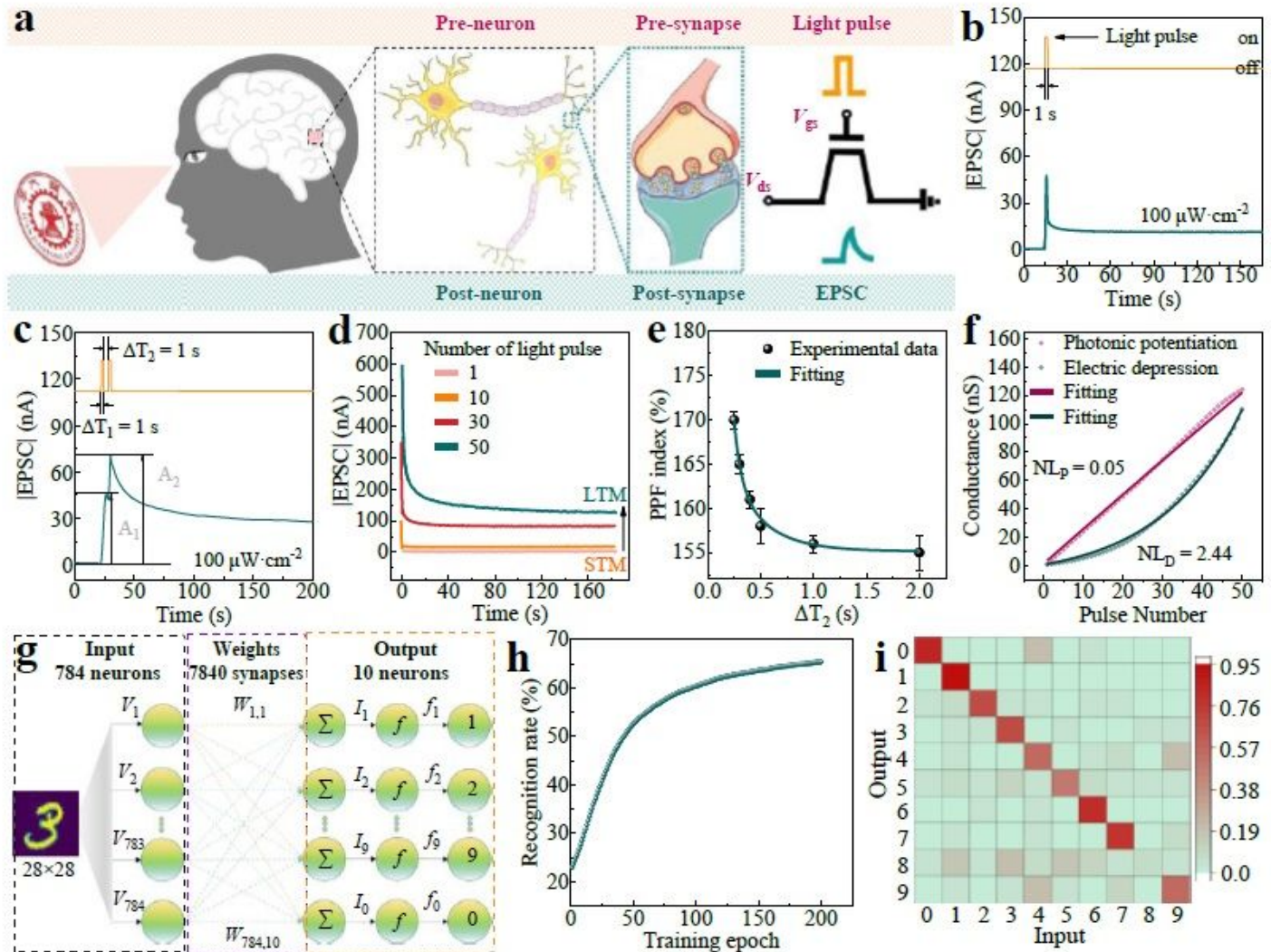

Figure 3

The photo-response of C8-BTBT-based OFETs with C8-PTCDI. a-b In-situ transfer curves by ozone treatment for a 0 s and b 600 s in the dark and under light intensity of 1 mW·cm−2, respectively. During the sweep of Vgs, the device was under light illumination. The abbreviation "1 w." denotes that the OFETs were placed in the open air with relative humidity 45% for 1 week after light illumination for 5 s. The abbreviation "C8-PTCDI (D)" denote the C8-PTCDI molecules were partially degraded by oxygen species, showing a degraded electrical performance. c Output curves of the OFETs in the dark and under fixed light intensity. d Transfer curves of the OFETs under different light intensities. e The dependence of ΔVon and Iphoto/Idark ratio on the ozone treatment time. f Fluorescence spectra of pure C8-BTBT film and C8-PTCDI/C8-BTBT (D) film excited at wavelength 365 nm. g The schematic diagram of the erasing process with the light wavelength of 365 nm through the hollowed plate mask with a "XJTU" pattern. The recorded light information of Iphoto/Idark ratio with "XJTU" pattern: h as-prepared, and i OFETs stored in open air with relative humidity 45% for 1 week. The OFETs were measured at Vds = -60 V. The thicknesses of C8-BTBT and C8-PTCDI thin films are 40 nm and 2 nm, respectively.

Figure 4

The role of degraded C8-PTCDI film as the organic n-type electrets for OFETs memories. a- b Transfer curves of OFETs based on 40 nm C8-BTBT with 2 nm C8-PTCDI after programming (Vgs = -100 V for 1 s)

and erasing (simultaneously applying Vgs = +100 V and light illumination with 1 mW·cm-2 for 1 s) processes. "Pro." and "Era." denote programming and erasing, respectively. The device in b was pre-treated by ozone for 600 s to obtain degraded C8-PTCDI. c The statistics of properties of electret-containing OFETs in term of charge densities of electret and field-effect mobilities. Detailed comparisons and references are provided in Supplementary Table 1. d-e Cycle repeatability for d and environmental stability for e after erasing. f Retention life time of organic memory device. According to b, the reading process was carried out at Von. It is noted that the OFETs were measured at Vds = -60 V.

Figure 5

Emulation of synaptic functions by the C8-BTBT/C8-PTCDI (D) artificial synaptic OFETs. a Scheme of a biological synapse and the C8-BTBT/C8-PTCDI (D) artificial synaptic OFETs. The skill of picture recognition by the human eye involves transmitting picture information through the retina to the visual cortex. Human body's mastery of skills is related to learning. Synapses connect neurons in the visual cortex of brain to each other, thus forming a neural network that can control the release of skills. b EPSC plot of the C8-BTBT/C8-PTCDI (D) artificial synaptic OFETs triggered by light spike (pulse width (ΔT): 1 s). c EPSC plot of the C8-BTBT/C8-PTCDI (D) artificial synaptic OFETs triggered by light spike (pulse

width (ΔT1): 1 s; spike time interval (ΔT2): 1 s). d Evolution of EPSC after stimulation by various numbers of light pulses. e Plots of extracted PPF index (A2/A1) versus spike time interval (ΔT2). A1 and A2 are the first and second EPSC peaks, respectively. The solid line is the fitted curve using double exponential function. f Schematic diagram of the applied photonic/electrical pulse sequence used to obtain the 50 weight states of synaptic devices. g Schematic diagram of an artificial neural network based on a single layer perceptron with 784 input neurons and 10 output neurons fully connected through 7840 synaptic weights. h Training function for the average recognition rate for 100 weight states, based on a MNIST test set of over 10,000 numbers from 0 to 9 in total. i Recognition capability of the artificial neural network. The diagonal of the matrix represents the recognition rate of 10 digits from 0-9, and the rest of the matrix represents the error rate. The artificial synaptic OFETs were measured at Vds = -5 V.

Supplementary Files

This is a list of supplementary files associated with this preprint. Click to download.

- SupplementaryInformation.pdf